Thermal stability and phase transformation of α-, κ(ε)-, and γ-Ga$_2$O$_3$ films under different ambient conditions ⊘

Jingyu Tang ✉ iD ; Kunyao Jiang iD ; Po-Sen Tseng iD ; Rachel C. Kurchin iD ; Lisa M. Porter iD ;
Robert F. Davis iD

Check for updates

CHORUS

View
Online

Export
Citation

Articles You May Be Interested In

Generalized mechanism for the solid phase transition of M$_2$O$_3$ (M=Al, Ga) featuring single cation migration and martensitic lattice transformation

Chin. J. Chem. Phys. (August 2024)

Unraveling the atomic mechanism of the disorder–order phase transition from γ-Ga$_2$O$_3$ to β-Ga$_2$O$_3$

APL Mater. (January 2024)

Thermal stability of HVPE-grown (0001) α-Ga$_2$O$_3$ on sapphire template under vacuum and atmospheric environments

J. Vac. Sci. Technol. A (May 2023)

Applied Physics Letters

AIP Publishing

Thermal stability and phase transformation of α-, $\kappa(\varepsilon)$-, and γ-Ga₂O₃ films under different ambient conditions

View Online   Export Citation   CrossMark

Jingyu Tang,[1,a] (iD) Kunyao Jiang,[1] (iD) Po-Sen Tseng,[1] (iD) Rachel C. Kurchin,[1] (iD) Lisa M. Porter,[1] (iD)
and Robert F. Davis[1,2] (iD)

AFFILIATIONS

[1]Department of Materials Science and Engineering, Carnegie Mellon University, Pittsburgh, Pennsylvania 15213, USA
[2]Department of Electrical and Computer Engineering, Carnegie Mellon University, Pittsburgh, Pennsylvania 15213, USA

[a]Author to whom correspondence should be addressed: jingyuta@andrew.cmu.edu

ABSTRACT

Phase transitions in metastable α-, $\kappa(\varepsilon)$-, and γ-Ga₂O₃ films to thermodynamically stable β-Ga₂O₃ during annealing in air, N₂, and vacuum have been systematically investigated via *in situ* high-temperature x-ray diffraction (HT-XRD) and scanning electron microscopy (SEM). These respective polymorphs exhibited thermal stability to $\sim$471–525 °C, $\sim$773–825 °C, and $\sim$490–575 °C before transforming into β-Ga₂O₃, across all tested ambient conditions. Particular crystallographic orientation relationships were observed before and after the phase transitions, i.e., (0001) α-Ga₂O₃ → $(\bar{2}01)$ β-Ga₂O₃, (001) $\kappa(\varepsilon)$-Ga₂O₃ → (310) and $(\bar{2}01)$ β-Ga₂O₃, and (100) γ-Ga₂O₃ → (100) β-Ga₂O₃. The phase transition of α-Ga₂O₃ to β-Ga₂O₃ resulted in catastrophic damage to the film and upheaval of the surface. The respective primary and possibly secondary causes of this damage are the +8.6% volume expansion and the dual displacive and reconstructive transformations that occur during this transition. The $\kappa(\varepsilon)$- and γ-Ga₂O₃ films converted to β-Ga₂O₃ via singular reconstructive transformations with small changes in volume and unchanged surface microstructures.

Published under an exclusive license by AIP Publishing. https://doi.org/10.1063/5.0214500

Gallium oxide (Ga₂O₃) occurs in four universally accepted polymorphs: α-(trigonal), β-(monoclinic), γ-(cubic-defective spinel), and $\kappa(\varepsilon)$–(orthorhombic) Ga₂O₃. The existence of a fifth polymorph, δ-Ga₂O₃, with a cubic-bixbyite structure remains under debate.[1] Among these polymorphs, β-Ga₂O₃ is the thermodynamically stable phase to its melting point; all other polymorphs convert to β-Ga₂O₃ when heated.[2] While β-Ga₂O₃ has attracted the most attention for its potential in high-power electronics and optoelectronics applications, the monoclinic symmetry of this polymorph creates anisotropy in its optical, electronic, and thermal properties.[3–6] As such, the metastable polymorphs, with their distinct crystal structures, symmetries, and properties, have recently garnered considerable interest.

α-Ga₂O₃ has the largest bandgap ($\sim$5.3 eV[7,8]) among all the polymorphs and is a promising alternative material for applications in high-power electronics, as indicated by its higher Baliga figure of merit relative to β-Ga₂O₃.[9] Electrical measurements of Schottky barrier diodes fabricated on α-Ga₂O₃ have shown a lower on-resistance of $\sim$0.1 mΩ·cm² (Ref. 10) compared with >0.32 mΩ·cm² for β-Ga₂O₃.[11,12] α-In₂O₃/α-Ga₂O₃ p-n junctions have also been

reported.[13,14] Moreover, the bandgap of α-Ga₂O₃ can be tuned via alloying with other oxides, such as Al₂O₃ and In₂O₃ (Refs. 9 and 15), that possess the same corundum structure. $\kappa(\varepsilon)$-Ga₂O₃ is also of considerable interest as it is the only polymorph that lacks inversion symmetry, meaning that spontaneous polarization is theoretically possible and this material could be piezoelectric (and possibly ferroelectric).[16,17] If ferroelectricity were to occur in $\kappa(\varepsilon)$-Ga₂O₃, the magnitude has been predicted to be an order of magnitude higher than in AlN and GaN.[18,19] Prior work on γ-Ga₂O₃ has indicated its potential utility in applications such as photoluminescence, catalytic and photocatalytic degradation of select organic compounds, and room-temperature ferromagnetism when incorporated with Mn.[20–22] For these and other applications, it is crucial to understand maximum operating temperatures for these metastable polymorphs, as well as the upper limits of the post-fabrication thermal treatments such as rapid thermal annealing of metal contacts and post-annealing after ion implantation for dopant activation.

Several studies have examined the thermal stability of α- and $\kappa(\varepsilon)$-Ga₂O₃ across varying film thicknesses and annealing processes,

including both *ex situ* and *in situ* methods along with different ramping/cooling rates and holding periods at specific temperatures.[23–27] In this Letter, a comprehensive analysis of the thermal stability of α-, κ(ε)-, and γ-Ga$_2$O$_3$ epitaxial films, maintained at a similar thickness and subjected to an identical *in situ* annealing sequence, was undertaken under three ambient conditions. The effect of the annealing environment on thermal stability and the evolution of surface morphologies are detailed for each polymorph.

The epitaxial films investigated in this Letter were α-Ga$_2$O$_3$ grown on (0001) sapphire via halide vapor phase epitaxy (HVPE) by Kyma Technologies, and κ(ε)- and γ-Ga$_2$O$_3$ grown on (0001) sapphire and (100) MgAl$_2$O$_4$ (spinel) substrates, respectively, via vertical, low-pressure, cold-wall metal-organic chemical vapor deposition (MOCVD). The details regarding the precursors and parameters employed for the growth of our κ(ε)- and γ-Ga$_2$O$_3$ films have been reported in previous publications.[28,29] High-resolution x-ray diffraction (HR-XRD) patterns of the as-grown films were acquired using a Panalytical X'pert Pro MPD x-ray diffractometer having a 4-crystal Ge ×(220) monochromator. HT-XRD patterns were recorded with a Malvern Panalytical Empyrean diffractometer (mirror optics) equipped with a HTK 16 N high-temperature (HT) chamber that can be heated to 1600 °C. The latter equipment was employed to observe phase transitions in our metastable polymorphs to β-Ga$_2$O$_3$ as a function of temperature in air, ultra-high purity (5 N) N$_2$ and vacuum (∼5 × 10^{-5} Torr). Each Ga$_2$O$_3$ film/substrate assembly was heated in increments of 100 °C and held at each temperature for 1 h while the XRD data were acquired. Heating in increments of 25 °C was applied near the phase transition temperature to observe the dynamics of this transition in each metastable polymorph. The ramping rate was set at

30 °C/min to 500 °C and reduced to 10 °C/min for higher temperatures. The cooling rate was set to be 30 °C/min. Before initiating *in situ* measurements in N$_2$, the HT-XRD chamber underwent five pump-and-purge cycles to ensure the elimination of residual gases. As discussed below, temperature calibration under vacuum was necessary after the measurement due to the changes in the modes of heating in this environment. Scanning electron microscopy (SEM) was performed to investigate the evolution of the surface morphology of the as-grown and post-annealed films for each polymorph.

Figures 1(a)–1(c) show 2θ-ω scans of α-Ga$_2$O$_3$, κ(ε)-Ga$_2$O$_3$, and γ-Ga$_2$O$_3$ films grown on c-plane sapphire, c-plane sapphire, and (100) MgAl$_2$O$_4$, respectively. Figure 1(b) reveals a shoulder near the (004) κ(ε)-Ga$_2$O$_3$ peak, attributed to the presence of ($\bar{4}$02) β-Ga$_2$O$_3$ within the film, a common observation for κ(ε)-Ga$_2$O$_3$ films grown by MOCVD.[28,30,31] β-Ga$_2$O$_3$ has been shown to be present near the film–substrate interface.[28,31] The optimized growth rate for κ(ε)-Ga$_2$O$_3$ is approximately 700 nm/h as reported in our previous publication.[28] It has been determined that the growth rate is a critical factor controlling the phases in the MOCVD process.[28,32] At a given temperature, higher growth rates favor the formation of metastable κ(ε)-Ga$_2$O$_3$ as the dominant phase in the films, while lower growth rates favor the formation of more thermally stable β-Ga$_2$O$_3$ as the dominant phase. Jinno *et al.*[24] reported a strong correlation between film thickness and thermal stability of α-Ga$_2$O$_3$ films deposited on c-plane sapphire; the thinner the film, the more stable upon heat treatment. To mitigate thickness and substrate-induced strain effects on thermal stability of our films, the thicknesses were maintained at ∼0.9 μm and confirmed to be in a relaxed state in reciprocal space maps (RSMs) shown in Figs. 1(d)–1(f). The separation of the vertical line passing through the center
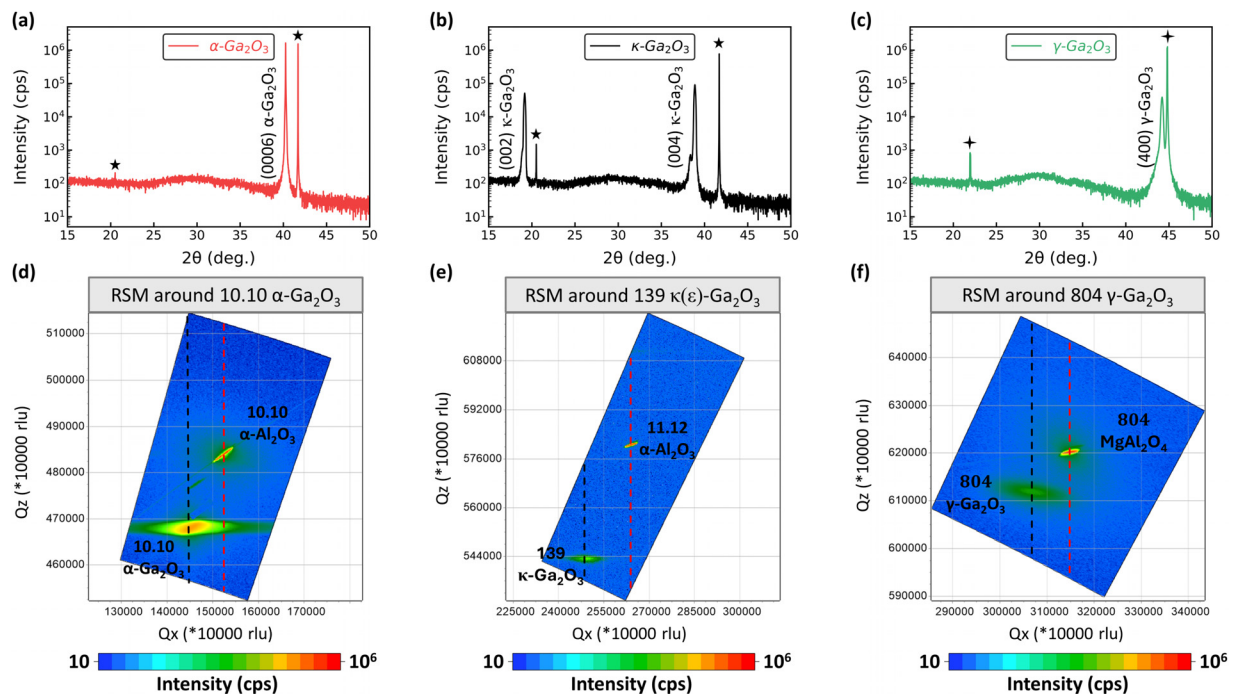
FIG. 1. High-resolution 2θ-ω scans displayed on a log scale for (a) α-Ga$_2$O$_3$ on c-sapphire, (b) κ(ε)-Ga$_2$O$_3$ on c-sapphire, and (c) γ-Ga$_2$O$_3$ on (100) MgAl$_2$O$_4$ as-grown films, and their associated RSMs in (d)–(f). The starred peaks in the x-ray patterns are from the respective substrates.
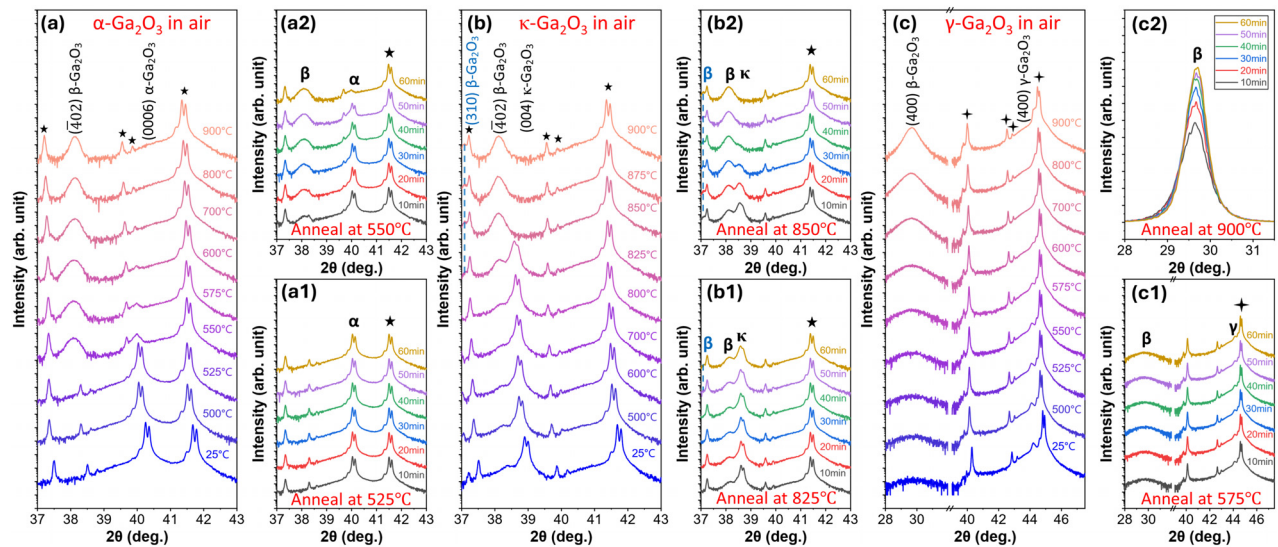
FIG. 2. HT-XRD 2θ-ω scans conducted in air for (a) α-Ga$_2$O$_3$ on c-sapphire, (b) $\kappa(\varepsilon)$-Ga$_2$O$_3$ on c-sapphire, and (c) γ-Ga$_2$O$_3$ on (100) MgAl$_2$O$_4$, respectively, in the temperature range of 500–900 °C. Note: (c2) has a narrower scanning range. The starred peaks in the x-ray patterns are from the respective substrates.

of the film spot (black dashed line) and substrate spot (red dashed line) indicates that these films were in a relaxed state.

Figure 2(a) shows the *in situ* HT-XRD patterns of α-Ga$_2$O$_3$ annealed in air in the temperature range from 500 °C to 900 °C. Note that all the diffracted peaks shifted to the left at elevated temperatures were due to thermal expansion (for more details see Fig. 4 and its accompanying description). These patterns reveal that (0001) oriented α-Ga$_2$O$_3$ maintains its thermal stability to 525 °C. However, a phase transition is initiated at ∼550 °C, which results in the formation of ($\bar{2}$01) oriented β-Ga$_2$O$_3$. The results of six consecutive scans for 10 min each conducted over 1 h annealing periods at both 525 °C and 550 °C are illustrated in Figs. 2(a1) and 2(a2), respectively. Notably, the α-Ga$_2$O$_3$ film annealed at 525 °C exhibits no detectable phase change, as evidenced by the nearly constant intensity of the (0006) α-Ga$_2$O$_3$ peak, depicted in Fig. 2(a1). In contrast, Fig. 2(a2) reveals a noticeable decrease in the intensity of the (0006) α-Ga$_2$O$_3$ peak accompanied by a gradual increase in the intensity of the ($\bar{4}$02) β-Ga$_2$O$_3$ peak for the film annealed at 550 °C. The α-Ga$_2$O$_3$ film is completely converted to β-Ga$_2$O$_3$ after annealing at 600 °C, because the α-Ga$_2$O$_3$ peak is no longer detectable and further increases in temperature do not affect the peak intensity of ($\bar{4}$02) β-Ga$_2$O$_3$. Wen *et al.*[23] determined using *in situ* HT-XRD that a 4 μm thick α-Ga$_2$O$_3$ grown on c-plane sapphire by HVPE was thermally stable up to 500–540 °C in air. Studies by other investigators[24,25] also demonstrated enhanced thermal stability of α-Ga$_2$O$_3$ beyond 600 °C via reduction of the film thickness to ∼100 nm on c- and m-plane sapphire.

Figure 2(b) presents the *in situ* HT-XRD patterns of $\kappa(\varepsilon)$-Ga$_2$O$_3$ annealed in air in the same temperature range from 500 °C to 900 °C. The (001) oriented $\kappa(\varepsilon)$-Ga$_2$O$_3$ was thermally stable to 800 °C, with a phase transition to both ($\bar{4}$02) and (310) oriented β-Ga$_2$O$_3$ starting around 825 °C. This transition is detailed in the six successive scans over a 1 h annealing period at both 825 °C and 850 °C, as shown in Figs. 2(b1) and 2(b2), respectively. Annealing at 825 °C resulted in a

gradual decrease in the intensity of the (004) $\kappa(\varepsilon)$-Ga$_2$O$_3$ peak and an increase in the intensity of both ($\bar{4}$02) and (310) β-Ga$_2$O$_3$ peaks toward the end of the 1 h annealing period, as shown in Fig. 2(b1). The transition occurred more rapidly for the film annealed at 850 °C [Fig. 2(b2)]. $\kappa(\varepsilon)$-Ga$_2$O$_3$ was completely converted to β-Ga$_2$O$_3$, as there was no detectable $\kappa(\varepsilon)$-Ga$_2$O$_3$ peak and no discernible increase in the peak intensity of either the ($\bar{4}$02) or the (310) β-Ga$_2$O$_3$ peaks when the temperature exceeded 850 °C. The coexistence of ($\bar{4}$02) and (310) β-Ga$_2$O$_3$ may be attributed to their similar oxygen sublattice atomic arrangements and lattice mismatches with (0001) α-Ga$_2$O$_3$. Studies by Fornari *et al.*[26] revealed that cooling $\kappa(\varepsilon)$-Ga$_2$O$_3$ films from 1000 °C at a rate of 7.5 °C/min and 2 °C/min resulted in the evolution of either the (310) or ($\bar{4}$02) peak, respectively, as the dominant β-Ga$_2$O$_3$ peak. Recently, Xu *et al.*[33] explored the competitive growth of the (310) and the ($\bar{4}$02) orientations of β-Ga$_2$O$_3$ grown on c-plane sapphire by HVPE. They noted the similarity of the atomic arrangements of these two planes and the c-plane of sapphire, and the effect of growth temperatures and HCl flow rates on the formation of the energetically unfavorable (310) oriented β-Ga$_2$O$_3$.

Figure 2(c) presents the *in situ* HT-XRD patterns of γ-Ga$_2$O$_3$ annealed in air within the aforementioned temperature range. The (100) oriented γ-Ga$_2$O$_3$ was determined to be thermally stable to 575 °C; however, a phase transition to (100) oriented β-Ga$_2$O$_3$ was initiated at ∼600 °C. This transition progressed more slowly than those observed for α- and $\kappa(\varepsilon)$-Ga$_2$O$_3$. Successive scans over 1 h annealing periods at 575 °C and 900 °C are shown in Figs. 2(c1) and 2(c2), respectively. The scans in Fig. 2(c1) exhibit no significant phase change, as evidenced by the nearly constant intensity of the (400) γ-Ga$_2$O$_3$ peak. The small lattice mismatch (∼+1.9%) between the γ-Ga$_2$O$_3$ film and the MgAl$_2$O$_4$ substrate, combined with the resolution limits of the XRD equipment, made it difficult to observe the (400) γ-Ga$_2$O$_3$ peak below 3600 cps, since the background intensity at the same 2θ position for a bare MgAl$_2$O$_4$ substrate is approximately
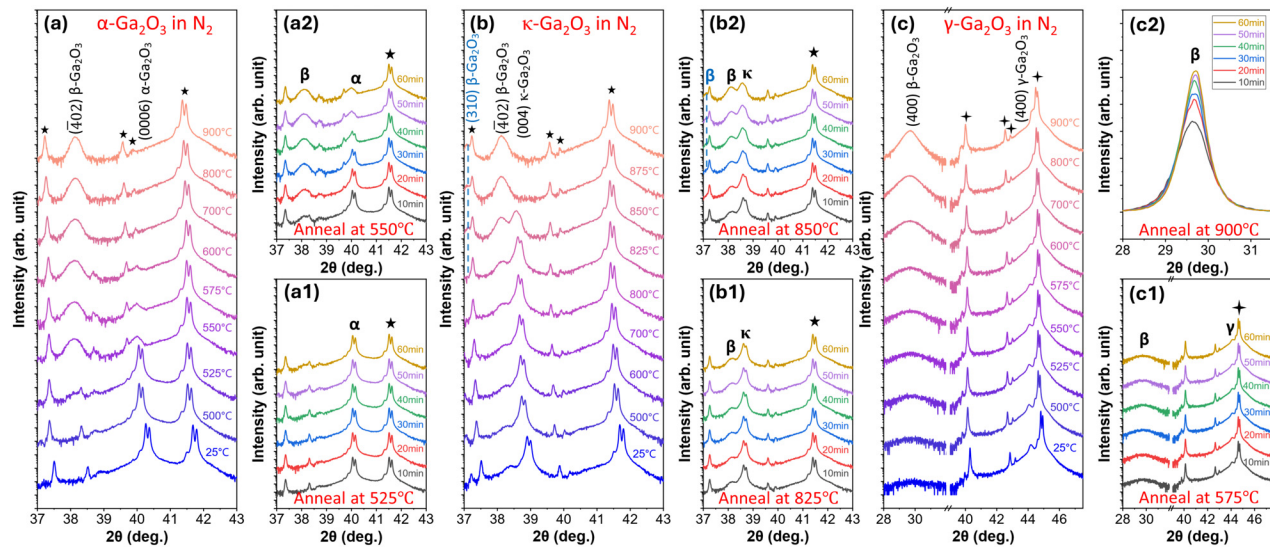
FIG. 3. HT-XRD 2θ-ω scans conducted in N_2 for (a) α-Ga_2O_3 on c-sapphire, (b) $\kappa(\varepsilon)$-Ga_2O_3 on c-sapphire, and (c) γ-Ga_2O_3 on (100) $MgAl_2O_4$, respectively, in the temperature range of 500–900 °C. The starred peaks in the x-ray patterns are from the respective substrates.

3600 cps. Therefore, no (400) γ-Ga_2O_3 peak can be detected when the intensity drops below the background and only the (400) β-Ga_2O_3 peak is used to study the phase transformation. Thus, the continued increase in the (400) β-Ga_2O_3 peak for the film annealed at 900 °C suggests an incomplete phase transition, as shown in Fig. 2(c2). Further increasing the annealing temperature to 1000 °C caused significant Mg and Al interatomic diffusion from the substrate into the film and resulted in the formation of γ-Ga_2O_3 solid solutions, as detailed in our earlier publications.[34,35]

Figures 3(a)–3(c) show the *in situ* HT-XRD patterns of α-Ga_2O_3, $\kappa(\varepsilon)$-Ga_2O_3, and γ-Ga_2O_3 films, respectively, annealed in N_2 within the temperature range of 500–900 °C. Similar to the observations made in air, the α-Ga_2O_3, $\kappa(\varepsilon)$-Ga_2O_3, and γ-Ga_2O_3 films were thermally stable to approximately 525 °C, 825 °C, and 575 °C, respectively. Almost no detectable decrease in the film peak intensities occurred during the 1 h annealing period at these temperatures, as shown in Figs. 3(a1)–3(c1). Lee *et al.*[27] reported that an α-Ga_2O_3 film with a thickness of ~720 nm was thermally stable to 550 °C in N_2. Fornari *et al.*[26] determined via *ex situ* annealing that phase transitions in 500 nm thick $\kappa(\varepsilon)$-Ga_2O_3 films occurred around 900 °C, in both O_2 and N_2 atmospheres.

The *in situ* HT-XRD experiments under vacuum were conducted with the sample temperature range from 110 °C to 865 °C based on the calibration process described below. The temperature difference between the platinum stage and the surface of the sapphire and spinel substrates was determined to be less than 20 °C when the stage temperature was below 900 °C in air and N_2. However, in conducting the same *in situ* measurements in vacuum, significant temperature differences were noted between the sample stage and the substrate because of the poor heat transfer in vacuum, likely due to lack of convection to the sample surface from the atmosphere. This observation was initially identified from the inconsistency in the calculated out-of-plane lattice constants of the sapphire and spinel substrates beneath the α-Ga_2O_3,

$\kappa(\varepsilon)$-Ga_2O_3, and γ-Ga_2O_3 films, in comparison to similar data acquired for these substrates heated in air and N_2, as shown in Figs. 4(a)–4(c). Temperature calibration in vacuum was done based on the second-order polynomial fit of the constant out-of-plane lattice vs temperature determined in air and N_2. Figures 4(d)–4(f) show a consistent out-of-plane lattice constant of the sapphire and spinel substrates vs calibrated temperature.

Figures 5(a)–5(c) present the *in situ* HT-XRD patterns of α-Ga_2O_3, $\kappa(\varepsilon)$-Ga_2O_3, and γ-Ga_2O_3 films annealed in vacuum from room temperature to ~900 °C. Consistent with findings in air and N_2, the thermal stabilities of α-Ga_2O_3, $\kappa(\varepsilon)$-Ga_2O_3, and γ-Ga_2O_3 films were maintained within the ranges of 471–490 °C, 773–818 °C, and 490–590 °C, respectively, as shown in Figs. 5(a1)–5(c1). As noted above, Wen *et al.*[23] conducted a similar HT-XRD study on α-Ga_2O_3 films grown on c-sapphire substrates and annealed within the temperature range of under a vacuum of 10^{-4} Torr. They observed that the phase transition to β-Ga_2O_3 occurred at 700 °C, a temperature 200 °C higher than annealing in air. This variation is thought to be attributed to the difference in oxygen partial pressures affecting oxygen diffusion. They surmised that the oxygen concentrations of the various intermediate GaO_x compositions decrease during the transformation with the decrease in pO_2 due to the reduction of oxygen diffusion. This phenomenon eventually increases the overall kinetic barrier for phase transformation. However, our results did not indicate a similar enhancement in thermal stability under vacuum in any of the three metastable polymorphs. We hypothesize that this may be related to the length of time the samples were held at each temperature. Wen *et al.* stabilized the sample for 5 min at each temperature before recording the data; we held the sample for 1 h, during which six successive scans were performed to verify whether the system had reached equilibrium.

Figure 6 displays SEM images of both as-grown and post-annealed α-Ga_2O_3, $\kappa(\varepsilon)$-Ga_2O_3, and γ-Ga_2O_3 films processed under
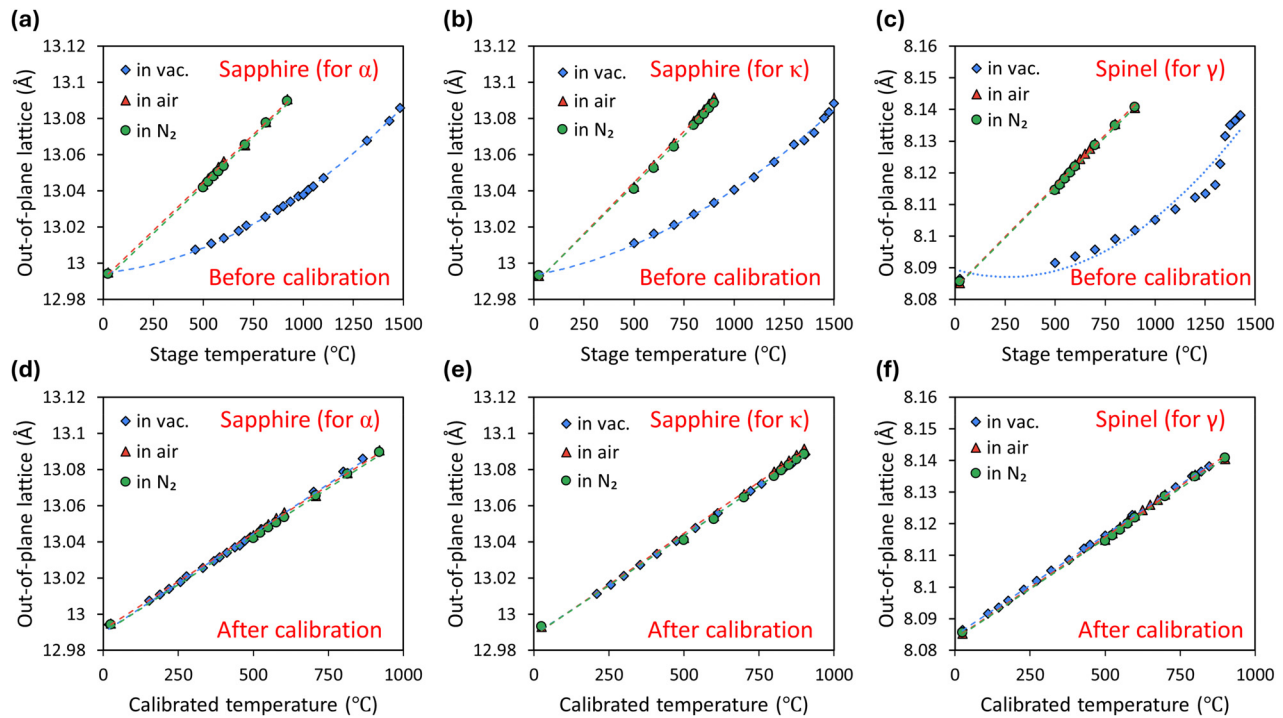
FIG. 4. Out-of-plane lattice constants vs stage or calibrated temperature for sapphire and spinel substrates in vacuum before and after calibration.
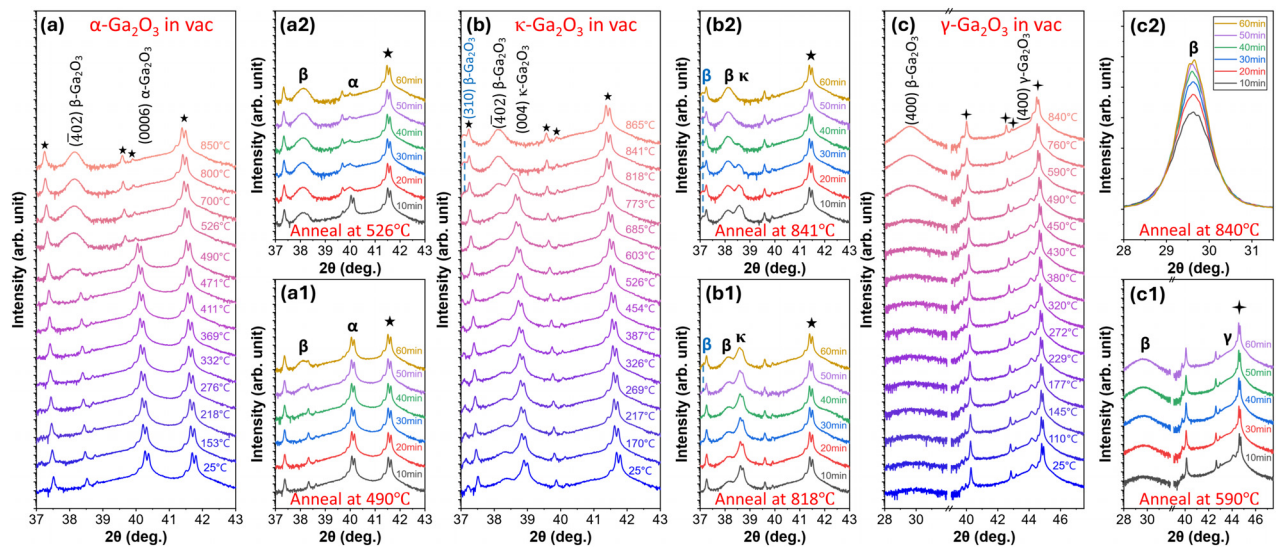

FIG. 5. HT-XRD 2θ-ω scans conducted in vacuum with a base pressure of 5×10^{-5} Torr for (a) α-Ga$_2$O$_3$ on c-sapphire, (b) $\kappa(\varepsilon)$-Ga$_2$O$_3$ on c-sapphire, and (c) γ-Ga$_2$O$_3$ on (100) MgAl$_2$O$_4$, respectively, in the calibrated temperature range of 110–865 °C. The starred peaks in the x-ray patterns are from the respective substrates.

various conditions. As detailed above, annealing the films resulted in their complete phase transformation into β-Ga$_2$O$_3$. Only the α-Ga$_2$O$_3$ films experienced a catastrophic phase transition characterized by widespread rupture and upheaval of the surface across the entire material regardless of the ambient conditions. A similar observation has

been reported in α-Ga$_2$O$_3$ films by Wen et al.[23] This phenomenon of marked film damage is similar to that observed during the θ-alumina (C2/m, structurally equivalent to β-Ga$_2$O$_3$) to α-alumina (R$\bar{3}$c, structurally equivalent to α-Ga$_2$O$_3$) phase transition. This latter transition has been attributed to a substantial volume reduction of
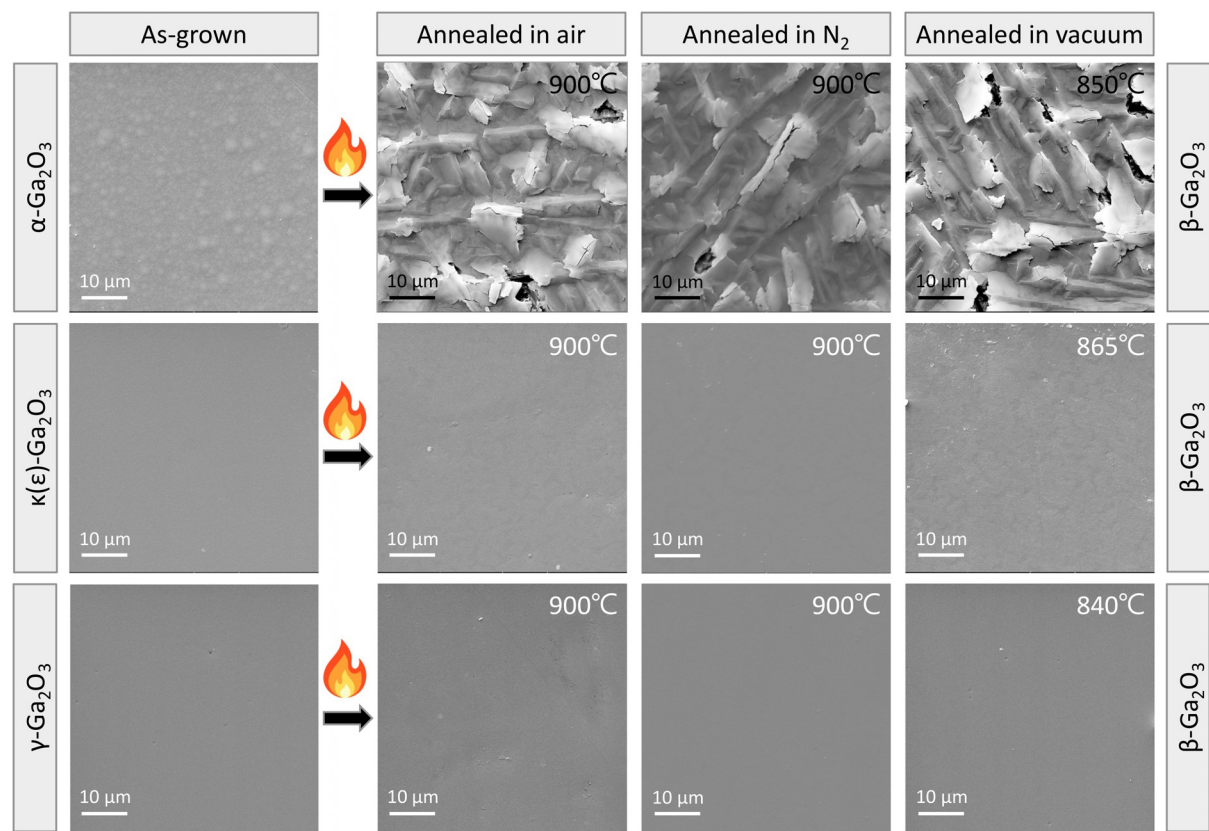
FIG. 6. SEM images of the α-Ga$_2$O$_3$, $\kappa(\varepsilon)$-Ga$_2$O$_3$, and γ-Ga$_2$O$_3$ films before and after annealing under different ambient conditions. All films converted to β-Ga$_2$O$_3$ by $\sim$900 °C.

$\sim$10 vol. %[36,37] during heating. In the case of the α- to β-Ga$_2$O$_3$ transition, a positive volume expansion of +8.6 vol. % is involved and is the primary cause of the severe film damage. In contrast, the $\kappa(\varepsilon)$-Ga$_2$O$_3$ and γ-Ga$_2$O$_3$ films maintained their surface morphologies after each phase transition in the three ambient conditions. The data presented in Table I provide a comparison of the change in volume of each metastable Ga$_2$O$_3$ phase in relation to β-Ga$_2$O$_3$ as well as the type of phase transition, density, and the oxygen sublattice arrangement in each phase. The transformation of α-Ga$_2$O$_3$ to β-Ga$_2$O$_3$ is both a displacive and a reconstructive phase transition, which is likely a secondary cause

of the disruption in the microstructure. The shearing of the oxygen sublattice from hexagonal close-packing (HCP) to face-centered cubic (FCC) packing is classified as a diffusionless displacive (martensitic) transition.[38] However, the relocation of gallium cations involves short-range diffusion and synchronized shear with the oxygen sublattice and is classified as a reconstructive transition.[38] By comparison, the oxygen sublattices for $\kappa(\varepsilon)$-Ga$_2$O$_3$ and γ-Ga$_2$O$_3$ are structurally similar to the oxygen sublattice in β-Ga$_2$O$_3$. The phase transitions in these two polymorphs primarily involve short-range diffusion and are thus reconstructive transitions. Theoretical studies on the transition from

TABLE I. Comparison of the density, change in volume at room temperature, and type of phase transition involved in the transformation of α-Ga$_2$O$_3$, $\kappa(\varepsilon)$-Ga$_2$O$_3$, and γ-Ga$_2$O$_3$ films to β-Ga$_2$O$_3$.

Phase	Density (g/cm^3)	Δ volume with respect to β (%)	O sublattice atomic arrangement	Phase transition type
α-Ga$_2$O$_3$	$\sim$6.453[40,41]	+8.6	2H(HCP)	Displacive + reconstructive[38]
$\kappa(\varepsilon)$-Ga$_2$O$_3$	$\sim$6.111[42,43]	+2.8	4H(HCP)	Reconstructive
γ-Ga$_2$O$_3$	$\sim$5.940[42,44]	−0.05	FCC	Reconstructive
β-Ga$_2$O$_3$	$\sim$5.943[45,46]	0	FCC	—

γ-Al$_2$O$_3$ (Fd$\bar{3}$m, structurally equivalent to γ-Ga$_2$O$_3$) to θ-alumina suggest it involves local migration of Al atoms without the shearing of the oxygen sublattice.[39] The volume changes associated with the phase transitions in $\kappa(\varepsilon)$-Ga$_2$O$_3$ and γ-Ga$_2$O$_3$ are much smaller than that in α-Ga$_2$O$_3$, as shown in Table I, and contribute markedly to the preservation of the surface morphology during the phase transition in each polymorph.

The thermal stability and phase evolution of structurally relaxed, $\sim$1 μm thick films of α-Ga$_2$O$_3$, $\kappa(\varepsilon)$-Ga$_2$O$_3$, and γ-Ga$_2$O$_3$ have been determined via in situ HT-XRD in air, N$_2$, and vacuum environments. These polymorphs exhibited stability against transformation to β-Ga$_2$O$_3$ up to $\sim$471–525 °C, $\sim$773–825 °C, and $\sim$490–575 °C, respectively, across all tested ambient conditions. Strong crystallographic orientation relationships were observed before and after the phase transitions, namely, (0001) α-Ga$_2$O$_3$ $\rightarrow$ ($\bar{2}$01) β-Ga$_2$O$_3$, (001) $\kappa(\varepsilon)$-Ga$_2$O$_3$ $\rightarrow$ (310) and ($\bar{2}$01) β-Ga$_2$O$_3$, and (100) γ-Ga$_2$O$_3$ $\rightarrow$ (100) β-Ga$_2$O$_3$. Notably, the α-Ga$_2$O$_3$ film experienced a catastrophic transformation characterized by severe rupture and upheaval of the surface under all ambient conditions and was primarily caused by the significant positive volume expansion during the transition. The changes in the arrangement of oxygen and gallium sublattices during the α-Ga$_2$O$_3$ to β-Ga$_2$O$_3$ transition are complex, involving both displacive and constructive transformations that likely played a secondary role in the disruption of the microstructure. They are also complex relative to the singular reconstructive transformations and much smaller volume changes that occur in the transitions of $\kappa(\varepsilon)$-Ga$_2$O$_3$ and γ-Ga$_2$O$_3$ films to β-Ga$_2$O$_3$.

AUTHOR DECLARATIONS
Conflict of Interest

The authors have no conflicts to disclose.

Author Contributions

Jingyu Tang: Conceptualization (equal); Data curation (equal); Formal analysis (equal); Investigation (equal); Methodology (equal); Validation (equal); Visualization (lead); Writing – original draft (lead). **Kunyao Jiang:** Conceptualization (equal); Data curation (equal); Formal analysis (equal); Investigation (equal); Methodology (equal); Validation (equal); Visualization (equal); Writing – review & editing (equal). **Po-Sen Tseng:** Data curation (equal); Visualization (equal); Writing – review & editing (equal). **Rachel C. Kurchin:** Methodology (equal); Supervision (equal); Writing – review & editing (lead). **Lisa M. Porter:** Funding acquisition (lead); Methodology (equal); Project administration (lead); Resources (lead); Supervision (lead); Writing – review & editing (lead). **Robert F. Davis:** Methodology (equal); Project administration (lead); Resources (lead); Supervision (lead); Writing – review & editing (lead).

DATA AVAILABILITY

The data that support the findings of this study are openly available in KiltHub at https://doi.org/10.1184/R1/26265200.v1, Ref. 47.

REFERENCES

[1] T. Kato, H. Nishinaka, K. Shimazoe, K. Kanegae, and M. Yoshimoto, "Demonstration of bixbyite-structured δ-Ga$_2$O$_3$ thin films using β-Fe$_2$O$_3$ buffer layers by mist chemical vapor deposition," ACS Appl. Electron. Mater. **5**(3), 1715–1720 (2023).

[2] R. Roy, V. G. Hill, and E. F. Osborn, "Polymorphism of Ga$_2$O$_3$ and the system Ga$_2$O$_3$–H$_2$O," J. Am. Chem. Soc. **74**(3), 719–722 (1952).

[3] K. Yamaguchi, "First principles study on electronic structure of β-Ga$_2$O$_3$," Solid State Commun. **131**(12), 739–744 (2004).

[4] Y. Zhang, J. Yan, G. Zhao, and W. Xie, "First-principles study on electronic structure and optical properties of Sn-doped β-Ga$_2$O$_3$," Physica B **405**(18), 3899–3903 (2010).

[5] N. Ueda, H. Hosono, R. Waseda, and H. Kawazoe, "Anisotropy of electrical and optical properties in β-Ga$_2$O$_3$ single crystals," Appl. Phys. Lett. **71**, 933–935 (1997).

[6] Z. Guo, A. Verma, X. Wu, F. Sun, A. Hickman, T. Masui, A. Kuramata, M. Higashiwaki, D. Jena, and T. Luo, "Anisotropic thermal conductivity in single crystal β-gallium oxide," Appl. Phys. Lett. **106**(11), 111909 (2015).

[7] D. Shinohara and S. Fujita, "Heteroepitaxy of corundum-structured α-Ga$_2$O$_3$ thin films on α-Al$_2$O$_3$ substrates by ultrasonic mist chemical vapor deposition," Jpn. J. Appl. Phys., Part 1 **47**, 7311–7313 (2008).

[8] A. Segura, L. Artús, R. Cuscó, R. Goldhahn, and M. Feneberg, "Band gap of corundumlike α-Ga$_2$O$_3$ determined by absorption and ellipsometry," Phys. Rev. Mater. **1**(2), 024604 (2017).

[9] Y. Oshima and E. Ahmadi, "Progress and challenges in the development of ultra-wide bandgap semiconductor α-Ga$_2$O$_3$ toward realizing power device applications," Appl. Phys. Lett. **121**(26), 260501 (2022).

[10] M. Oda, R. Tokuda, H. Kambara, T. Tanikawa, T. Sasaki, and T. Hitora, "Schottky barrier diodes of corundum-structured gallium oxide showing on-resistance of 0.1mΩ·cm^2 grown by MIST EPITAXY®," Appl. Phys. Express **9**(2), 021101 (2016).

[11] S. Roy, A. Bhattacharyya, P. Ranga, H. Splawn, J. Leach, and S. Krishnamoorthy, "High-k oxide field-plated vertical (001) β-Ga$_2$O$_3$ Schottky barrier diode with Baliga's figure of merit over 1 GW/cm^2," IEEE Electron Device Lett. **42**, 1140 (2021).

[12] K. Konishi, K. Goto, H. Murakami, Y. Kumagai, A. Kuramata, S. Yamakoshi, and M. Higashiwaki, "1-kV vertical Ga$_2$O$_3$ field-plated Schottky barrier diodes," Appl. Phys. Lett. **110**(10), 103506 (2017).

[13] S. Kan, S. Takemoto, K. Kaneko, I. Takahashi, M. Sugimoto, T. Shinohe, and S. Fujita, "Electrical properties of α-Ir$_2$O$_3$/α-Ga$_2$O$_3$ pn heterojunction diode and band alignment of the heterostructure," Appl. Phys. Lett. **113**(21), 212104 (2018).

[14] K. Kaneko, Y. Masuda, S. I. Kan, I. Takahashi, Y. Kato, T. Shinohe, and S. Fujita, "Ultra-wide bandgap corundum-structured p-type α-(Ir,Ga)$_2$O$_3$ alloys for α-Ga$_2$O$_3$ electronics," Appl. Phys. Lett. **118**(10), 102104 (2021).

[15] S. Fujita and K. Kaneko, "Epitaxial growth of corundum-structured wide band gap III-oxide semiconductor thin films," J. Cryst. Growth **401**, 588–592 (2014).

[16] F. He, K. Jiang, Y. Choi, B. L. Aronson, S. Shetty, J. Tang, B. Liu, Y. Liu, K. P. Kelley, G. B. Rayner, R. F. Davis, L. M. Porter, and S. Trolier-McKinstry, "High field dielectric response in κ-Ga$_2$O$_3$ films," J. Appl. Phys. **134**(20), 204101 (2023).

[17] S. Yusa, D. Oka, and T. Fukumura, "High-κ dielectric ε-Ga$_2$O$_3$ stabilized in a transparent heteroepitaxial structure grown by mist CVD at atmospheric pressure," CrystEngComm **22**, 381–385 (2020).

[18] K. Shimada, "First-principles study of crystal structure, elastic stiffness constants, piezoelectric constants, and spontaneous polarization of orthorhombic Pna2$_1$-M$_2$O$_3$ (M = Al, Ga, In, Sc, Y)," Mater. Res. Express **5**(3), 036502 (2018).

[19] M. B. Maccioni and V. Fiorentini, "Phase diagram and polarization of stable phases of (Ga$_{1-x}$In$_x$)$_2$O$_3$," Appl. Phys. Express **9**(4), 041102 (2016).

[20]V. Devthade, A. Gupta, and S. S. Umare, "Graphitic carbon nitride-γ-gallium oxide (GCN-γ-Ga$_2$O$_3$) nanohybrid photocatalyst for dinitrogen fixation and pollutant decomposition," ACS Appl. Nano Mater. **1**(10), 5581–5588 (2018).

[21]T. Wang, S. S. Farvid, M. Abulikemu, and P. V. Radovanovic, "Size-tunable phosphorescence in colloidal metastable γ-Ga$_2$O$_3$ nanocrystals," J. Am. Chem. Soc. **132**(27), 9250–9252 (2010).

[22]H. Hayashi, R. Huang, H. Ikeno, F. Oba, S. Yoshioka, I. Tanaka, and S. Sonoda, "Room temperature ferromagnetism in Mn-doped γ-Ga$_2$O$_3$ with spinel structure," Appl. Phys. Lett. **89**(18), 181903 (2006).

[23]Z. Wen, K. Khan, K. Sun, R. Wellen, Y. Oshima, and E. Ahmadi, "Thermal stability of HVPE-grown (0001) α-Ga$_2$O$_3$ on sapphire template under vacuum and atmospheric environments," J. Vac. Sci. Technol. A **41**(4), 043403 (2023).

[24]R. Jinno, K. Kaneko, and S. Fujita, "Thermal stability of α-Ga$_2$O$_3$ films grown on c-plane sapphire substrates via mist-CVD," AIP Adv. **10**(11), 115013 (2020).

[25]J. P. McCandless, C. S. Chang, K. Nomoto, J. Casamento, V. Protasenko, P. Vogt, D. Rowe, K. Gann, S. T. Ho, W. Li, R. Jinno, Y. Cho, A. J. Green, K. D. Chabak, D. G. Schlom, M. O. Thompson, D. A. Muller, H. G. Xing, and D. Jena, "Thermal stability of epitaxial α-Ga$_2$O$_3$ and (Al,Ga)$_2$O$_3$ layers on m-plane sapphire," Appl. Phys. Lett. **119**(6), 062102 (2021).

[26]R. Fornari, M. Pavesi, V. Montedoro, D. Klimm, F. Mezzadri, I. Cora, B. Pécz, F. Boschi, A. Parisini, A. Baraldi, C. Ferrari, E. Gombia, and M. Bosi, "Thermal stability of ε-Ga$_2$O$_3$ polymorph," Acta Mater. **140**, 411–416 (2017).

[27]S. D. Lee, K. Akaiwa, and S. Fujita, "Thermal stability of single crystalline alpha gallium oxide films on sapphire substrates," Phys. Status Solidi C **10**(11), 1592–1595 (2013).

[28]K. Jiang, J. Tang, M. J. Cabral, A. Park, L. Gu, R. F. Davis, and L. M. Porter, "Layered phase composition and microstructure of κ-Ga$_2$O$_3$-dominant heteroepitaxial films grown via MOCVD," J. Appl. Phys. **131**(5), 055305 (2022).

[29]J. Tang, K. Jiang, C. Xu, M. J. Cabral, K. Xiao, L. M. Porter, and R. F. Davis, "Atomic-scale investigation of γ-Ga$_2$O$_3$ deposited on MgAl$_2$O$_4$ and its relationship with β-Ga$_2$O$_3$," APL Mater. **12**(1), 011109 (2024).

[30]Y. Zhuo, Z. Chen, W. Tu, X. Ma, Y. Pei, and G. Wang, "β-Ga$_2$O$_3$ versus ε-Ga$_2$O$_3$: Control of the crystal phase composition of gallium oxide thin film prepared by metal-organic chemical vapor deposition," Appl. Surf. Sci. **420**, 802–807 (2017).

[31]A. Hassa, C. Wouters, M. Kneiß, D. Splith, C. Sturm, H. V. Wenckstern, M. Albrecht, M. Lorenz, and M. Grundmann, "Control of phase formation of (Al$_x$Ga$_{1-x}$)$_2$O$_3$ thin films on c-plane Al$_2$O$_3$," J. Phys. D: Appl. Phys. **53**, 485105 (2020).

[32]M. Bosi, L. Seravalli, P. Mazzolini, F. Mezzadri, and R. Fornari, "Thermodynamic and kinetic effects on the nucleation and growth of ε/κ- or β-Ga$_2$O$_3$ by metal–organic vapor phase epitaxy," Cryst. Growth Des. **21**(11), 6393 (2021).

[33]W. Xu, Y. Li, B. Li, X. Xiu, H. Zhao, Z. Xie, T. Tao, P. Chen, B. Liu, R. Zhang, and Y. Zheng, "(3 $\bar{1}$ 0)-Oriented β-Ga$_2$O$_3$ grown on (0001) sapphire by halide vapor phase epitaxy: Growth and structural characterizations," CrystEngComm **25**, 6044–6049 (2023).

[34]J. Tang, K. Jiang, S. D. House, C. Xu, K. Xiao, L. M. Porter, and R. F. Davis, "Mg and Al-induced phase transformation and stabilization of Ga$_2$O$_3$-based γ-phase spinels," Appl. Phys. Lett. **123**(1), 012103 (2023).

[35]K. Jiang, J. Tang, C. Xu, K. Xiao, R. F. Davis, and L. M. Porter, "Evolution of β-Ga$_2$O$_3$ to γ-Ga$_2$O$_3$ solid-solution epitaxial films after high-temperature annealing," J. Vac. Sci. Technol. A **41**(6), 062702 (2023).

[36]P. Y. Hou, A. P. Paulikas, and B. W. Veal, "Growth strains and stress relaxation in alumina scales during high temperature oxidation," Mater. Sci. Forum **461-464**, 671–680 (2004).

[37]Y. Huang, X. Peng, and X. Q. Chen, "The mechanism of θ- to α-Al$_2$O$_3$ phase transformation," J. Alloys Compd. **863**, 158666 (2021).

[38]S. C. Zhu, S. H. Guan, and Z. P. Liu, "Mechanism and microstructures in Ga$_2$O$_3$ pseudomartensitic solid phase transition," Phys. Chem. Chem. Phys. **18**, 18563–18574 (2016).

[39]S. H. Cai, S. N. Rashkeev, S. T. Pantelides, and K. Sohlberg, "Atomic scale mechanism of the transformation of γ-alumina to θ-alumina," Phys. Rev. Lett. **89**(23), 235501 (2002).

[40]M. Marezuo and J. P. Remeika, "Bond lengths in the α-Ga$_2$O$_3$ structure and the high-pressure phase of Ga$_{2-x}$Fe$_x$O$_3$," J. Chem. Phys. **46**(5), 1862–1865 (1967).

[41]L. J. Eckert and R. C. Bradt, "Thermal expansion of alpha Ga$_2$O$_3$," J. Am. Ceram. Soc. **56**(4), 229–230 (1973).

[42]H. Y. Playford, A. C. Hannon, E. R. Barney, and R. I. Walton, "Structures of uncharacterised polymorphs of gallium oxide from total neutron diffraction," Chem.—Eur. J. **19**(8), 2803–2813 (2013).

[43]I. Cora, F. Mezzadri, F. Boschi, M. Bosi, M. Čaplovičová, G. Calestani, I. Dódony, B. Pécz, and R. Fornari, "The real structure of ε-Ga$_2$O$_3$ and its relation to κ-phase," CrystEngComm **19**, 1509–1516 (2017).

[44]M. Zinkevich, F. M. Morales, H. Nitsche, M. Ahrens, M. Rühle, and F. Aldinger, "Microstructural and thermodynamic study of γ-Ga$_2$O$_3$," Z. Metallkd. **95**, 756–762 (2004).

[45]H. Wang, Y. He, W. Chen, Y. W. Zeng, K. Stahl, T. Kikegawa, and J. Z. Jiang, "High-pressure behavior of β-Ga$_2$O$_3$ nanocrystals," J. Appl. Phys. **107**(3), 033520 (2010).

[46]F. Orlandi, F. Mezzadri, G. Calestani, F. Boschi, and R. Fornari, "Thermal expansion coefficients of β-Ga$_2$O$_3$ single crystals," Appl. Phys. Express **8**(11), 111101 (2015).

[47]Figshare. (2024). "In-situ XRD annealing 2theta-omega scans," KiltHub. https://doi.org/10.1184/R1/26265200.v1